Technical Note

Platform for Transport Aircraft Wing–Body Parametric Modeling and High-Lift System Design

Yun Tian[1]; Xiangnan Qu[2]; Peiqing Liu[3]; and Shiwei Yan, Ph.D.[4]

Abstract: In this paper, the authors describe a software they have developed for wing–body parametric modeling and high-lift system design. This software has the following features: (1) it generates and modifies geometric as well as aerodynamic analysis in the conceptual and preliminary aircraft design phases; (2) it integrates high-fidelity computer-aided design (CAD) and computational fluid dynamics (CFD) software by a graphical user interface(GUI); and (3) it has an aerodynamic/mechanical integrated design and kinematic simulation for a three-dimensional (3D) high-lift device. Based on the application program interface (API) techniques of specialized third-party software, the software integrates B-spline fitting and modeling of airfoil and complex curves, modeling of the fuselage and wings, a high-lift system design, the automatic generation of a structured grid, and high-fidelity CFD code based on Reynolds-averaged Navier–Stokes (RANS) equations. First, the geometry of the fuselage and wing is parametrically generated by lofting with control curves, and then the initial graphics exchange specification (IGES) format geometry is exported to an automatic grid generation module. Finally, the structured grid file is exported to the CFD solver for aerodynamic analysis. The NACA0012 airfoil and DLR-F6 FX2B wing–body model that was published at a workshop are selected for software validation. The cruise configuration model (with nacelle, wingtip, and empennage designed manually) of a 150 seat airliner designed using this software was subsequently used for a high-lift aerodynamic/mechanical integrated design and kinematic simulation. The results illustrate that the software was able to integrate wing–body modeling and high-lift aerodynamic/mechanism design in the conceptual and preliminary aircraft design phases. **DOI: 10.1061/(ASCE)AS.1943-5525.0000761.** © *2017 American Society of Civil Engineers.*

Introduction

The design of modern aircraft requires multidisciplinary analysis, including aerodynamic, structural mechanical, weight, cost, and safety analyses (Manning et al. 2004). To make the design process more efficient, it is important to properly integrate analysis methods and tools into the design process. Analysis results must be provided quickly and accurately when the input geometry is updated. Further, the level of detail in the model must match the fidelity requirements of the analysis in question.

Many software packages support the geometric shape design process for air vehicles around the world, for example, *AAA* (Anemaat and Schueler 1997), *RDS* (Head et al. 1992), and ACSYNT (Jayaram et al. 1992) from the U.S.; PIANO (Fidanci et al. 2000) and *Visual CAPDA* (Xie and Haberland 1999) from Europe; and *CADS* and *OpenCADS* from China (Lu and Gong 2008). These software packages can quickly achieve shape parametric modeling but cannot provide results in the standard graphics interchange format used by computer-aided design (CAD). Hence, CAD model building cannot be modified via CAD software, which immediately causes an inconvenience for subsequent detailed design phases. For these reasons, secondary development based on popular CAD software appeared. Yu Xiong Qing from the Nanjing University of Aeronautics and Astronautics developed parametric modeling of wing–body and flying–wing vehicles and then applied it to multidisciplinary design optimization (Zhan et al. 2009). With the rapid development of computer technology, the application of high-fidelity Reynolds-averaged Navier–Stokes (RANS) simulation technology in the conceptual and preliminary phases of aircraft design is no longer out of reach.

This paper presents a software for wing–body parametric modeling and high-lift system design, which was developed using VB 6.0 (Liu 2010). Based on the application program interface (API) technique of CATIA, the software integrates B-spline fitting and modeling of airfoil and complex curves, modeling of the fuselage and wings, high-lift system design, automatic generation of a structured grid, and a high-fidelity computational fluid dynamics (CFD) solver based on RANS. First, the geometry of the fuselage and wing is parametrically generated by lofting with control curves, and then the Initial Graphics Exchange Specification (IGES) format geometry is output to the automatic grid generation module. Next, the structured grid file is output to the CFD code for aerodynamic computation. The NACA0012 airfoil and wing–body of a DLR-F6 WB FX2B model published in the third *Drag Prediction Workshop* were used for software validation. The cruise wing–body geometry created earlier was subsequently used for a high-lift aerodynamic/mechanical integrated design and kinematic simulation. With the constraint of the kinematic system, a 3D high-lift system geometry shape was created, and the motion simulation module drove the high-lift devices to takeoff or landing positions.

[1]Lecturer, National Laboratory for Aeronautics and Astronautics, Beihang Univ., Beijing 100191, People's Republic of China. E-mail: aircraft@buaa.edu.cn

[2]Master, School of Aeronautic Science and Engineering, Beihang Univ., Beijing 100191, People's Republic of China. E-mail: qxiangnan@163.com

[3]Professor, School of Aeronautic Science and Engineering, Beihang Univ., Beijing 100191, People's Republic of China (corresponding author). E-mail: lpq@buaa.edu.cn

[4]Dept. of Surface Ship, China Marine Development and Research Center, Beijing 100164, People's Republic of China. E-mail: 2365215@163.com

Note. This manuscript was submitted on March 26, 2016; approved on March 6, 2017; published online on July 14, 2017. Discussion period open until December 14, 2017; separate discussions must be submitted for individual papers. This technical note is part of the ***Journal of Aerospace Engineering***, © ASCE, ISSN 0893-1321.

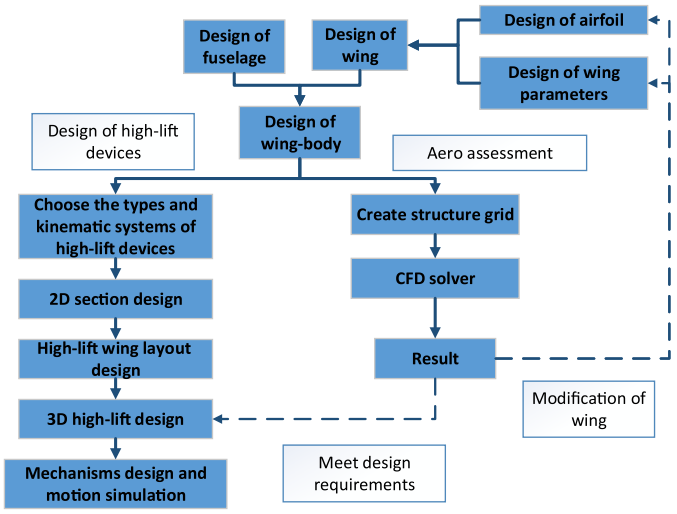

Fig. 1. Framework of our software

Software Framework

The software, which the researchers developed using VB 6.0, involves parametric modeling and the design of control curves (i.e., airfoils), fuselage design, wing design, CFD analysis of the airfoil and wing–body combination, and an aerodynamic/mechanical integrated design for a 3D high-lift device.

Fig. 1 shows the framework of the software, which consists of the following six modules: control curve (i.e., airfoil) parametric modeling, fuselage design, wing design, automatic grid generation, aerodynamic analysis, and high-lift system design. The high-lift system design is in turn formed by three submodules, i.e., two-dimensional (2D) section design, high-lift layout design, and 3D high-lift design. The control curves (i.e., airfoils) are fitted via B-spline, while the fuselage design adopts a lofting technique by a series of control curves which imported from external data files. The wing layout parameters can be used to confirm the position of the control airfoil and then create a clean wing in a similar way. The wing–body model, which is integrated with a clean wing and fuselage, is saved as an IGES format file; then the standard digital model outputs to an automatic grid generation module. Thus, a structured grid is generated by calling grid-generation tools, such as *ICEM* or *Pointwise* software. The grid file is then output to the RANS solver.

The CFD results (such as pressure, lift, and drag coefficients) can be used manually as feedback to modify the control curve (i.e., airfoil) and wing layout parameters such that the geometrical shape can be quickly updated. The high-lift system design is based on the clean wing–body geometry. First, the high-lift device types and kinematic system were selected. Then the 2D high-lift profile was designed. Next, the high-lift wing layout was designed and a 3D high-lift system geometric model to represent both take-off and landing statuses was created. Finally, the mechanisms to simulate the motion of high-lift devices were designed and assembled.

Parametric Modeling of Control Curves (i.e., Airfoils)

The fuselage section control curves and wing section control airfoils are used to generate the fuselage and wing geometry shape. The parametric method can be used to quickly modify the curves of the shape, thereby satisfying the requirements for fast updates of fuselage and wing geometry shape. In this work, a B-spline approach, be described next, was selected to fit the control curves.

From Shi (2001), a B-spline curve of pth degree is defined as

$$C(u) = \sum_{i=0}^{n} N_{i,p}(u) P_i, \qquad u_p \le u \le u_{n+1} \tag{1}$$

Here, $\{P_i | 0 \le i \le n\} \subset \mathbb{R}^d$ = control points sequenced on a plane (i.e., $d = 2$) or in 3D space (i.e., $d = 3$); and $U = \{u_0, u_1, \ldots, u_{n+p+1}\}$ = incremental sequence of real numbers called the knot vector. The basis function $N_{i,p}(u)$ is defined as

$$N_{i,0}(u) = \begin{cases} 1, & u_i \le u < u_{i+1} \\ 0, & \text{otherwise} \end{cases} \tag{2}$$

$$N_{i,p}(u) = \frac{u - u_i}{u_{i+p} - u_i} N_{i,p-1}(u) + \frac{u_{i+p+1} - u}{u_{i+p+1} - u_{i+1}} N_{i+1,p-1}(u) \tag{3}$$

Here, a specific value of 0/0 to be equal to zero was set.

The base airfoil and fuselage control sections are data files containing hundreds of data points. The control points of these curves are generated by interpolating or fitting these data points using B-spline interpolation. The accuracy of the parametric results is highest when the number of control points is equal to the number of data points by global interpolation; however, too many control points create obstacles to curve parameterization. Studies have shown that by using the nonuniform rational B-spline (NURBS) curve method to fit any airfoil, at least 13 control points are needed to achieve geometric approximation accuracy (Painchaud-Ouellet et al. 2004). A suitable number of control points can strike a good balance between accuracy and efficiency with B-spline fitting; moreover, the algorithm is relatively simple.

For the cubic B-spline basis function, there is

$$\boldsymbol{N}_j = [N_{j,3}(\overline{u_0}), N_{j,3}(\overline{u_1}), \ldots, N_{j,3}(\overline{u_m})]^T, \quad (j = 0, 1, \ldots, n) \tag{4}$$

$$\boldsymbol{A} = [\boldsymbol{N}_0, \boldsymbol{N}_1, \ldots, \boldsymbol{N}_n] \tag{5}$$

$$\boldsymbol{y} = (\overline{P_0}, \overline{P_1}, \ldots, \overline{P_m})^T \tag{6}$$

$$\boldsymbol{c} = (P_0, P_1, \ldots, P_n)^T \tag{7}$$

Here, $\{\bar{u}_k\}$ = knot set corresponding to data-point set $\{\overline{P_i}(x_i, y_i, z_i) | 0 \le i \le m\}$, obtained via centripetal parameterization. Note that $\{\bar{u}_k\}$ affects the shape of the curve and parameterization. Eq. (7) is decided by the normal equation $\boldsymbol{A}^T\boldsymbol{A}\boldsymbol{c}^* = \boldsymbol{A}^T\boldsymbol{y}$, which transforms Eq. (1) into the best square approximation B-spline curve of the data-point set $\{\overline{P_i}(x_i, y_i, z_i) | 0 \le i \le m\}$.

Based on the principle of least squares, this method obtains the optimal solution by solving a system of linear equations with the given dimension equal to the number of B-spline curve control points. When the number of control points exceeds 50, the average fitting error and maximum partial error of all data points can be controlled by on the order of 10^{-4} airfoil chords. Increasing the number of B-spline curve control points can improve the fitting precision; however, in consideration of the economy of the algorithm, a large number of control points is not necessary. Considering the fitting accuracy and efficiency, the number of control points was selected in the 15–50 range.

Fig. 2 shows the interface of the control section curve parameterization module. First, the original curve data from a data file

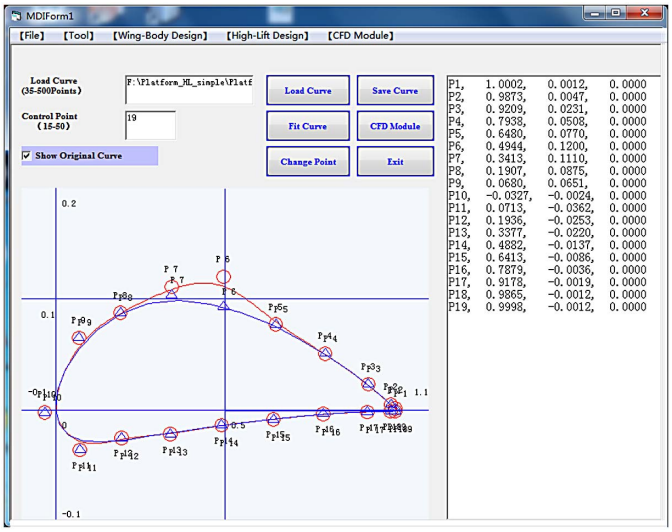

Fig. 2. Interface of control section curve parameterization module

was imported and the number of control points was specified. Second, the coordinates of the control points can be calculated by fitting the curve data according to the aforementioned B-spline method, and the image and coordinates of those control points can be directly displayed on the interface. Finally, the designer can modify the coordinates of some control points manually according to her experience and CFD results.

Fuselage and Wing Modeling

The parameters corresponding to the fuselage in the aircraft shape design process primarily consist of the length of the fuselage, equivalent diameter, fuselage slenderness ratio, control nodes of each transverse cross section, and fitting form of the transverse and vertical cross-section curves, for example. The parameters of the wing shape design primarily consist of, for example, the wing area, taper ratio, aspect ratio, sweepback angle, relative thickness of the airfoil, installation position of the wing, twist angle, and dihedral angle. Fig. 3 shows the interface of the fuselage and wing modeling module. The design of the wing needs to input a series of airfoils, with the spatial position of each airfoil calculated by the sweepback angle, dihedral angle, installation position, and twist angle. The leading edge line of the wing is straight in this platform. First, the spatial position of the leading-edge line can be defined by the sweepback angle, dihedral angle, and installation position. Second, the leading-edge points of different spanwise airfoils are fixed at the leading-edge line of the wing, and those airfoils are laid out by streamline and twist around the leading-edge point. Finally, those airfoils are used to loft the wing.

The shape of the fuselage is simpler than that of the wing, mainly because the shape of the fuselage is essentially cylindrical with contraction at the nose and tail. To obtain the geometric shape of the fuselage by lofting, the shape and position of each control cross-section curve of the fuselage must be defined, and the two guide curves are the connecting line of the start and end points of each section curve. Fig. 4 shows fuselage shaping using 13 control curves and wing shaping using 11 control airfoils.

After the wing and fuselage are generated, the location of the fuselage can be fixed according to the aircraft-body coordinate frame. The location of the wing can be fixed by the

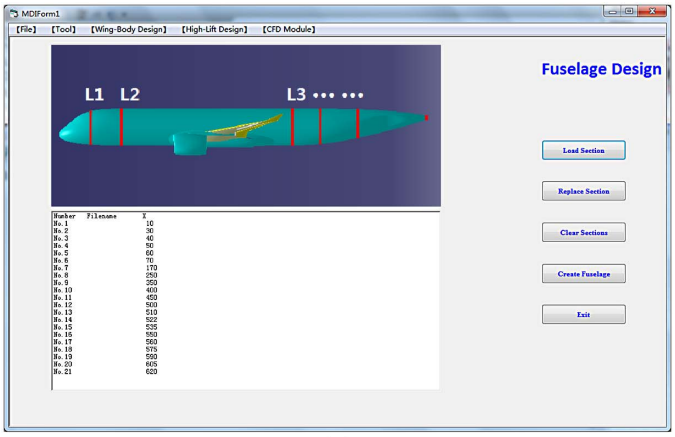

(a)

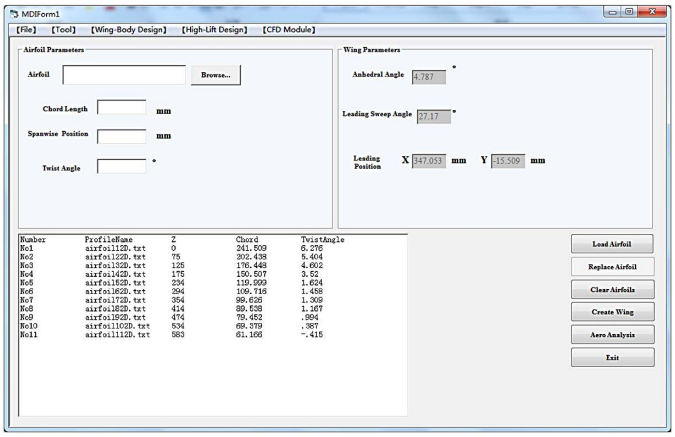

(b)

Fig. 3. (a) Fuselage modeling interface; (b) wing modeling interface

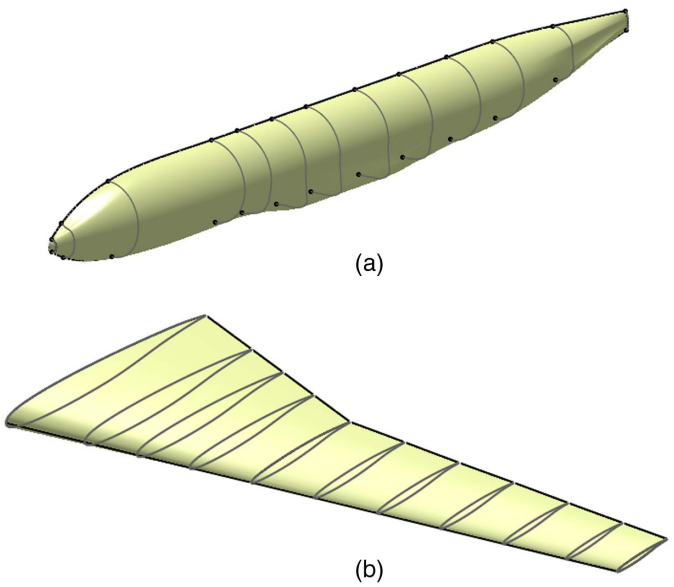

(a)

(b)

Fig. 4. (a) Fuselage shape; (b) wing shape

leading-edge point of the wing root, which is located in the aircraft symmetry plane (XY plane), and the wing can be translated by modifying the x or y-coordinates of the leading-edge point of wing root.

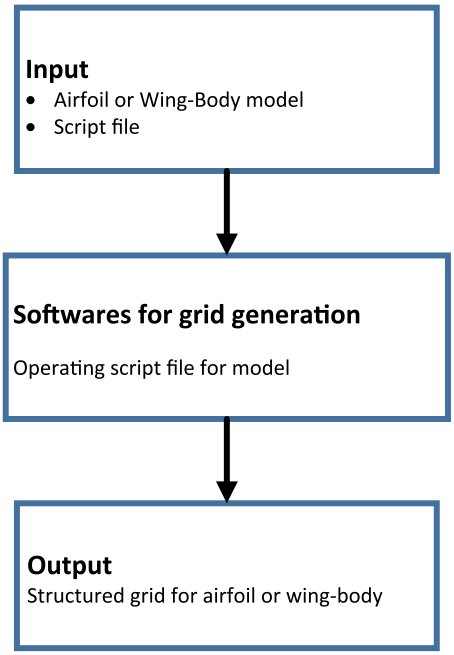

Fig. 5. Process illustrating automatic grid generation

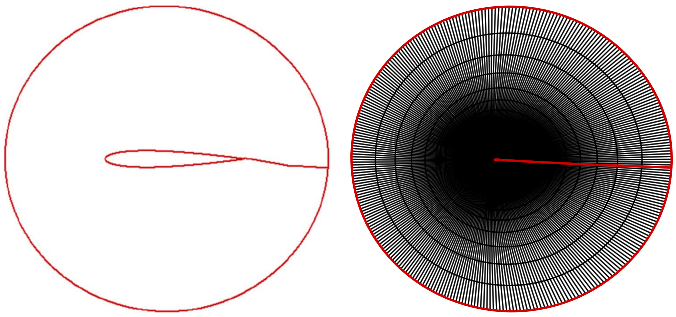

Fig. 6. Airfoil grid topology

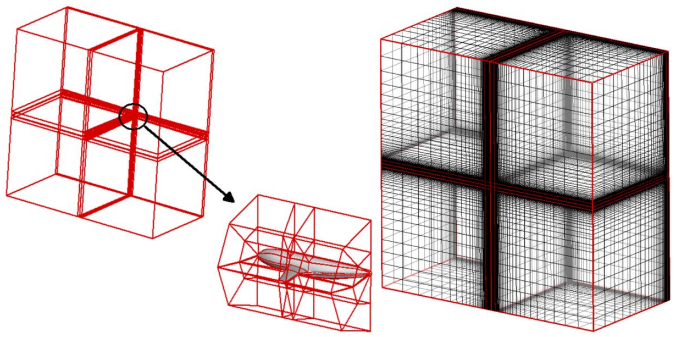

Fig. 7. Wing–body grid topology (by ICEM automatic grid generation script)

Automatic Generation of Structured Grid and the Aerodynamics Analysis Module

Illustrated in Fig. 5, the software integrates a function to automatically generate a structured grid for the airfoil and wing–body geometry. Here, *ICEM* or *Pointwise* provides a scripting language to help generate the grid. Further, modifying the airfoil and the geometry

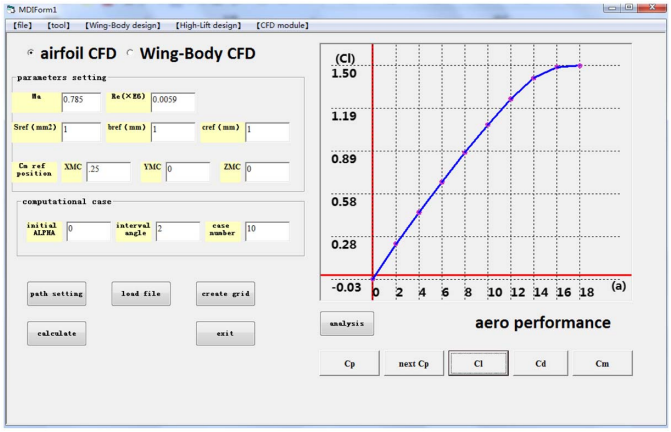

Fig. 8. Interface of aerodynamic performance analysis module of this software

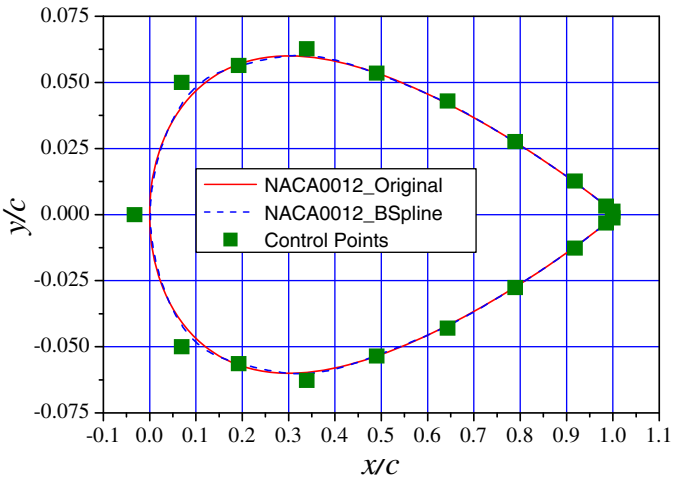

Fig. 9. B-spline fitting airfoil generated by 19 control points

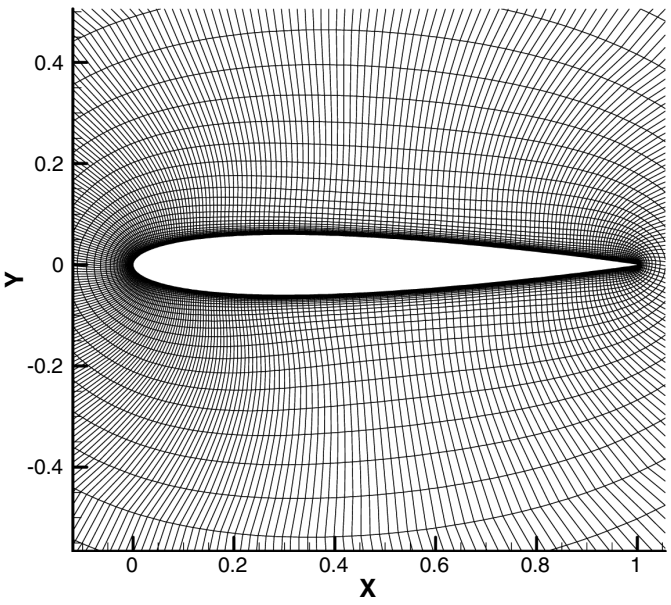

Fig. 10. NACA0012 airfoil grid

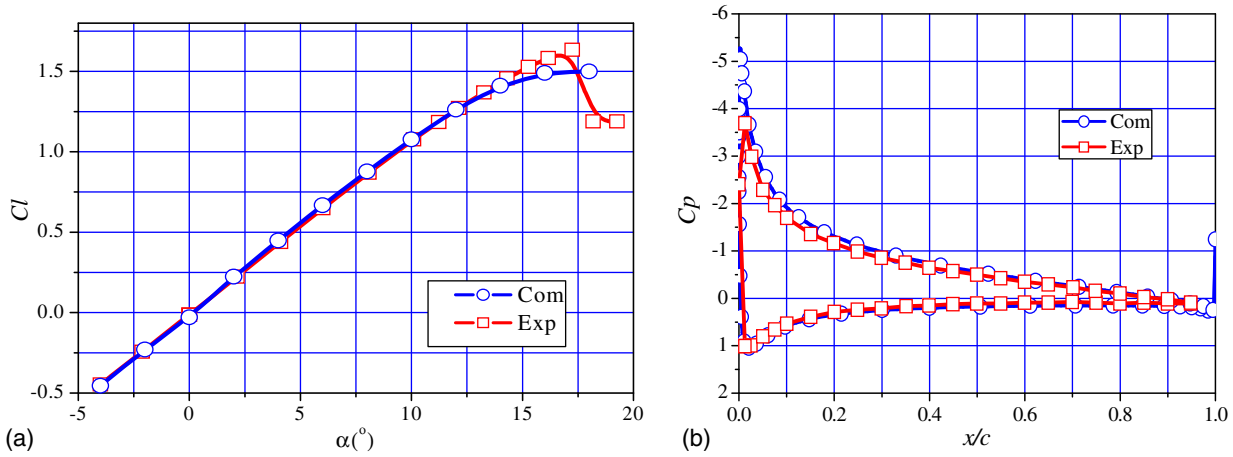

Fig. 11. (a) Comparison of lift coefficient; (b) comparison of pressure coefficients at $\alpha = 10°$

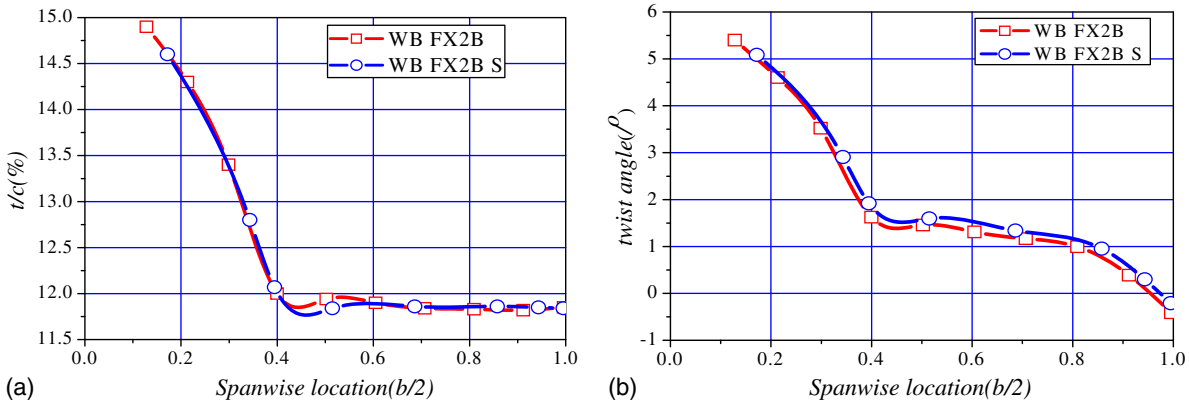

Fig. 12. (a) Variation of relative thickness; (b) variation of twist angle

model is an iterative process. For the efficiency of the design process, the grid-generation process is recorded via scripting, with the script files operable by *ICEM* or *Pointwise* to quickly generate a multiblock structured grid. Because of the minor modifications to the airfoil and wing–body model, the grid generated by the given script files can adjust to automatically map the model, as depicted in Figs. 6 and 7. The script files are recorded by hand based on a general 150 seat airliner wing–body model, and the user can replace the script file by a new one if the aircraft geometry and layout changed dramatically. Instead, this function is integrated into the process of aerodynamic analysis, illustrated in Fig. 8.

The software integrates *OpenFOAM* (Field Operation and Manipulation) solver for airfoil and wing–body aerodynamic analysis. The aerodynamic analysis interface is displayed in Fig. 8. Here, the CFD case can be quickly calculated after aerodynamic parameters and operating conditions are input via the interface. The flow solver is based on the RANS equation; by default, the turbulence model is one equation, the Spalart–Allmaras (SA) model, and the gas type is ideal.

Case Verification

Airfoil Case Verification

The numerical computation method regarding the airfoil using the NACA0012 airfoil was verified. Based on Wang (2013), the accuracy was acceptable with 19 control points to fit the NACA0012 airfoil. Fig. 9 compares the fitted airfoil created by the software with 19 control points (NACA0012_BSpline) and the original airfoil (NACA0012_Original). The NACA0012_BSpline airfoil coincides with the original airfoil, except for the nose. The accuracy of fitting can be improved by increasing the number of control points.

The numerical computation results of the NACA0012 original airfoil were compared with the experimental data. The 2D structured grid generated by the automatic generation module is shown

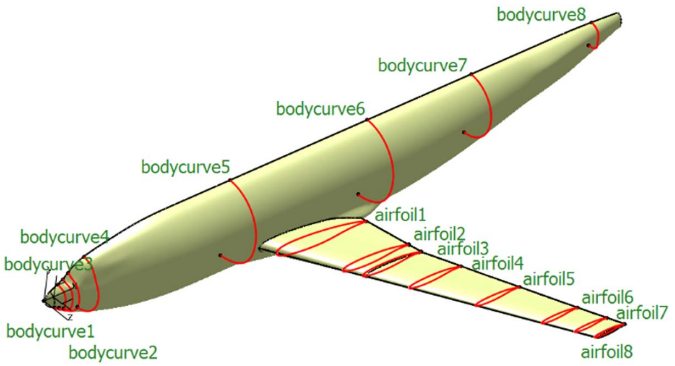

Fig. 13. Cross sections of fuselage and wing

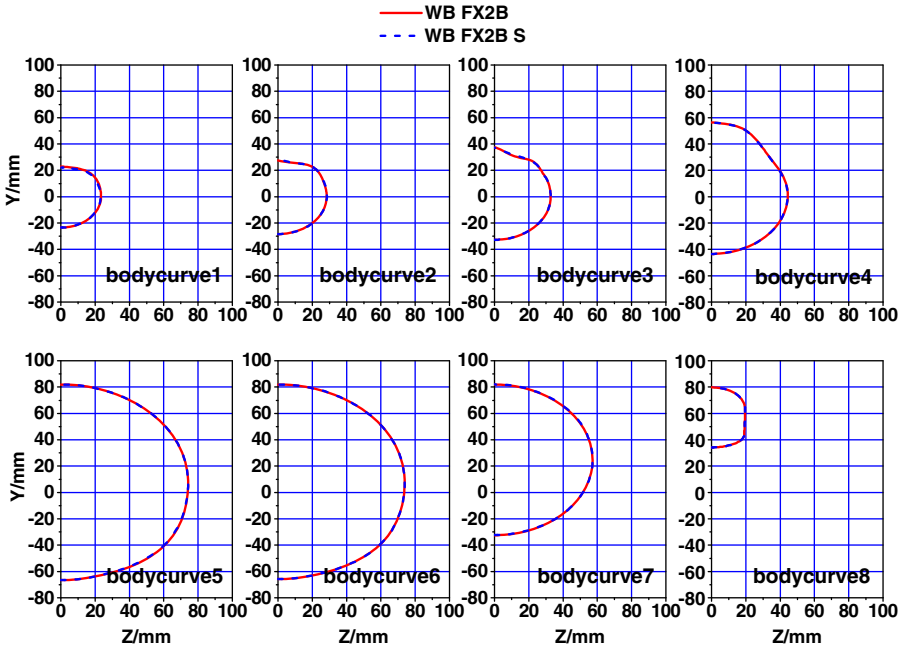

Fig. 14. Streamwise comparison of cross sections of fuselage

in Fig. 10. The grid size is approximately 4×10^4 cells, with the first cell size set to $5 \times 10^{-5}c$, freestream Mach number $\mathrm{M} = 0.1$, and Reynolds number $\mathrm{R} = 0.6 \times 10^6$. Fig. 11 compares C_L and C_P at $\alpha = 10°$. The C_L at the linear part (i.e., α from -4 to 12°) conformed to the experimental data quite well. Similar to C_L, C_P at $\alpha = 10°$ is faithful except at the nose because the experimental data are sparse.

Wing–Body Case Verification

The accuracy of modeling and numerical computation is verified by a wing–body model of DLR-F6 WB FX2B. The spanwise variations in the relative thickness and twist angle of the geometric model generated by this software (i.e., WB FX2B S) and the original model (i.e., WB FX2B) are shown in Fig. 12. There are differences between the original and new geometry primarily because the

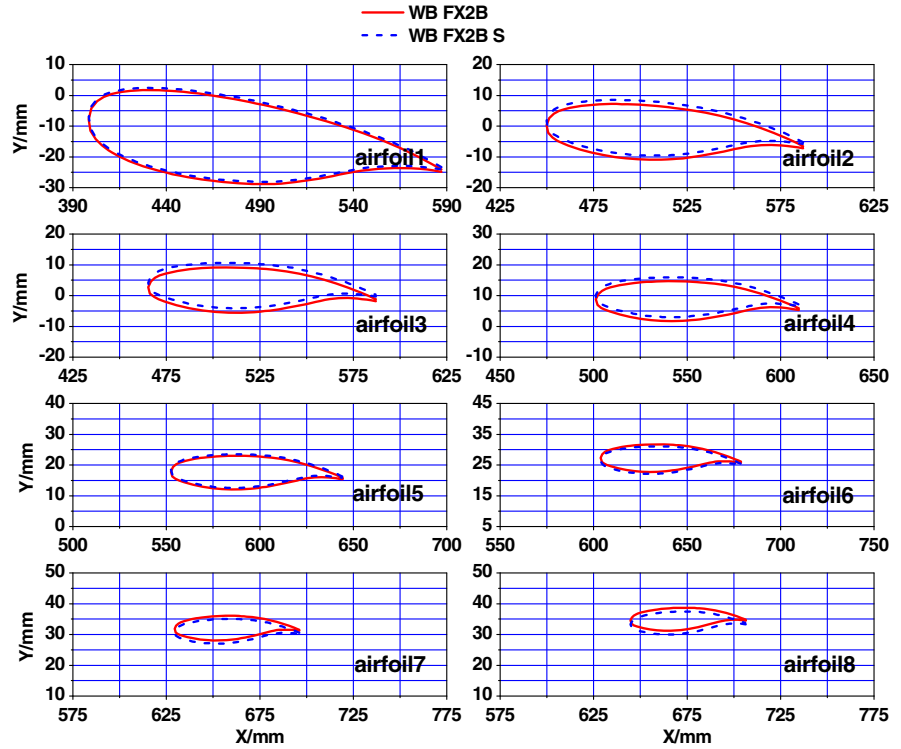

Fig. 15. Spanwise comparison of cross sections of wing

J. Aerosp. Eng., 2017, 30(5): 06017004

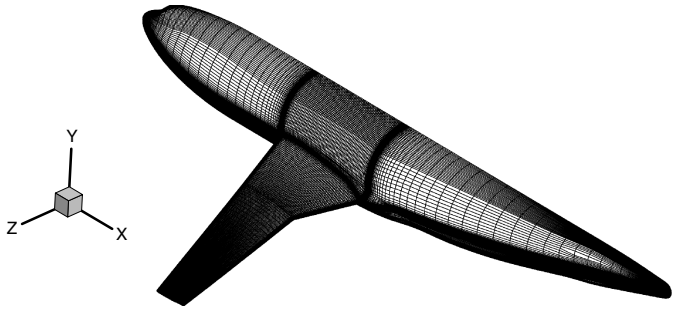

Fig. 16. Surface grid of wing–body model

leading edge of the original model wing is not straight, making the control airfoils rotate around the quarter-chord line. In practice, the result of wing modeling can thus be considered acceptable.

Both these parameters coincide well with those of WB FX2B S and WB FX2B. Eight cross sections are transected from the fuselage and wing respectively at the same position of WB FX2B S and WB FX2B (Fig. 13).

Figs. 14 and 15 illustrate the accuracy of the cross sections of the fuselage and wing, respectively. The accuracy of the fuselage sections is higher than that of the wing sections because the fuselage construction line is straight.

The aerodynamic performance of WB FX2B S and WB FX2B is analyzed and compared under the same computation method and grid, as shown in Fig. 16. Here, a multiblock structured grid is created. More specifically, an O-block is created on the surface, with the first cell size set to $4.25 \times 10^{-6}c$ and the grid size being approximately six million. The freestream condition is set to $\mathrm{M} = 0.75$ and $\mathrm{R} = 5 \times 10^{6}$.

To verify the numerical accuracy, the results were compared with computational results from Sclafani et al. (2008). The lift, drag, pitching-moment characteristic, and spanwise pressure coefficient results for $C_L = 0.5$ are presented in Figs. 17 and 18. The computational results of WB FX2B coincide well with the results from Sclafani et al. (2008). This comparison illustrates that the numerical accuracy of the wing–body model is reliable.

The aerodynamic characteristics of WB FX2B S and WB FX2B are also compared in Figs. 17 and 18. As shown in Fig. 17, the C_L, C_D, and C_M of WB FX2B S are higher than those of WB FX2B. Fig. 18 shows the spanwise variations of C_P between WB FX2B and WB FX2B S. The C_P deviation of the inboard wing is higher than that of the outboard wing because of the difference in geometric shape. In practice, the software can be considered reliable as a tool of geometric shape design and aerodynamic analysis in the phase of aircraft conceptual and preliminary design.

Aerodynamic/Mechanical Integrated Design of High-Lift System

The traditional design process of a high-lift system is shown in Fig. 19. The process is divided into a preliminary design phase, a design finalization phase, and a flight testing phase (Zhang 2002).

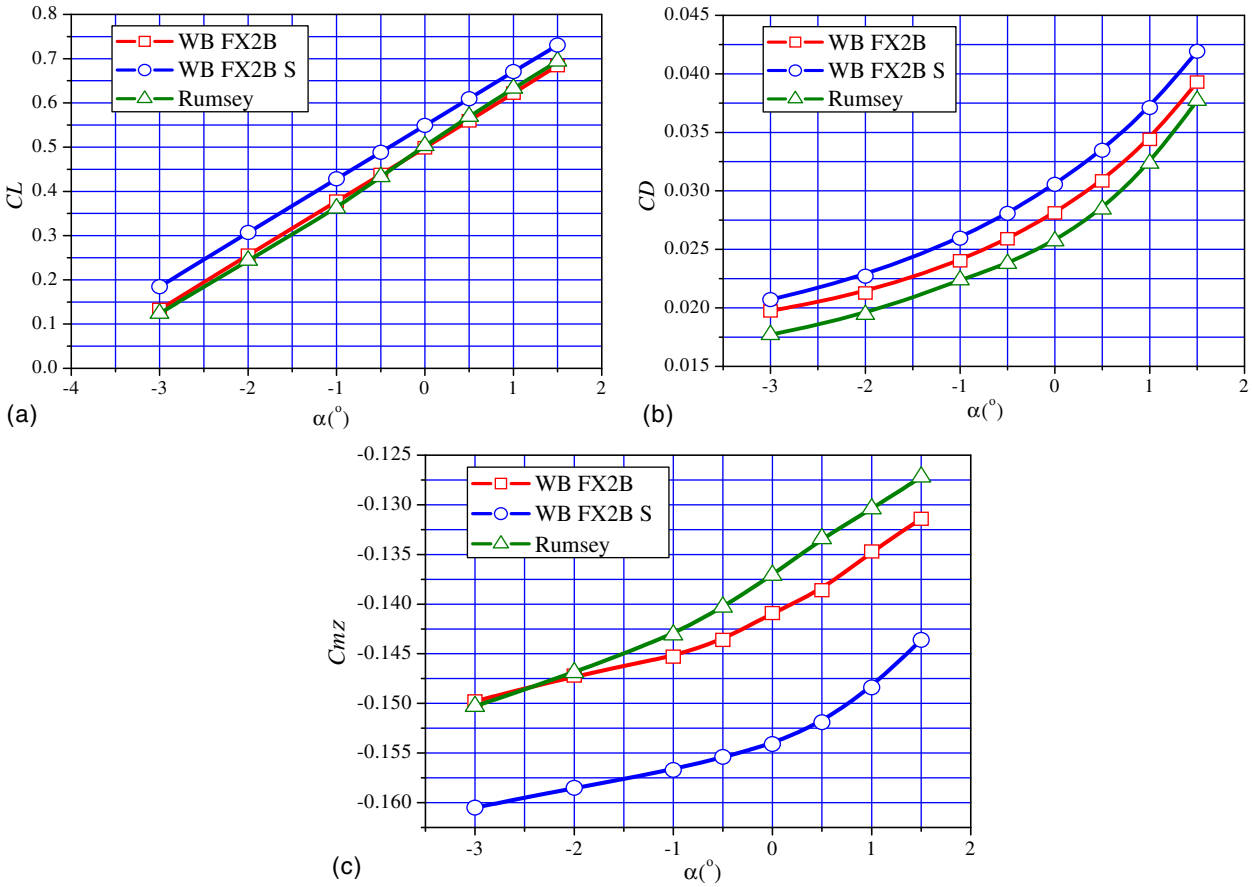

Fig. 17. (a) Comparison of lift coefficient; (b) comparison of drag coefficient; (c) comparison of pitching moment coefficient

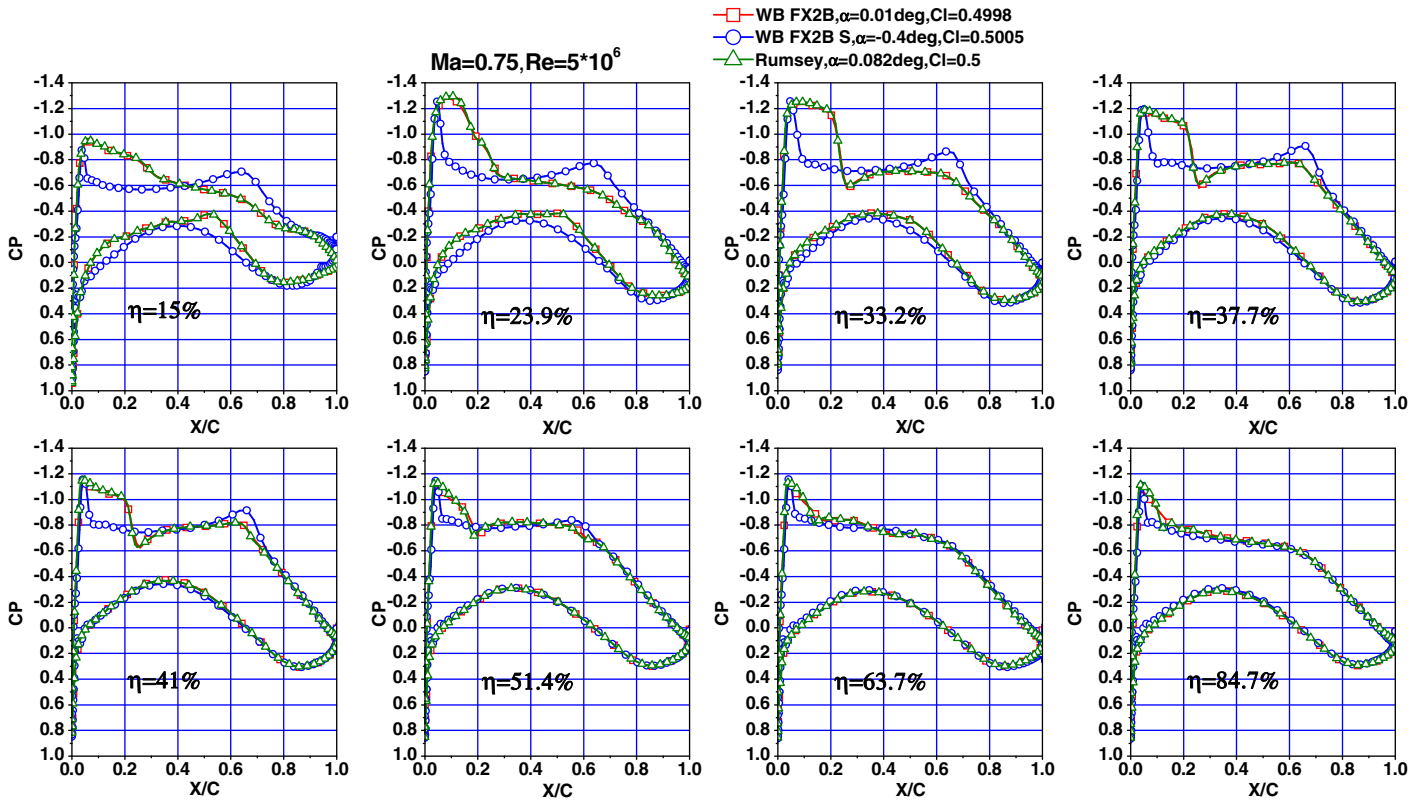

Fig. 18. Spanwise variations of pressure coefficients

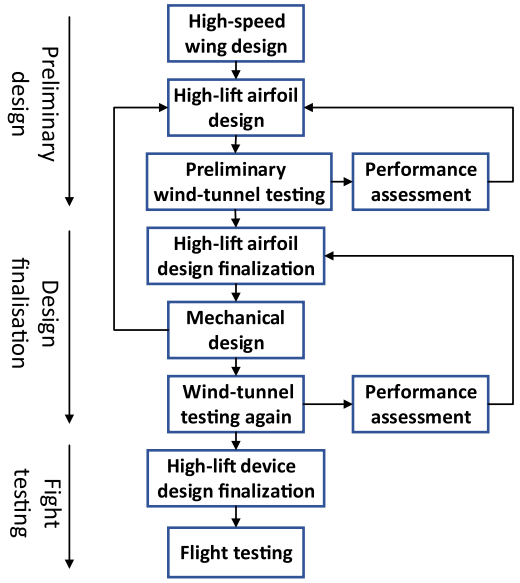

Fig. 19. Traditional design process of high-lift system

During the high-lift device preliminary design phase, one must determine the design objectives and what types of the high-lift device should be initially selected based on the requirements of takeoff, landing, and climbing performance. Then the high-lift device layout parameters based on the wing layout should be determined, including the relative chord length, relative spanwise length, and location of leading- and trailing-edge high-lift device. Finally, optimize the 2D multielement airfoils based on the wing. Taking into account the fact that the design of the high-lift device is

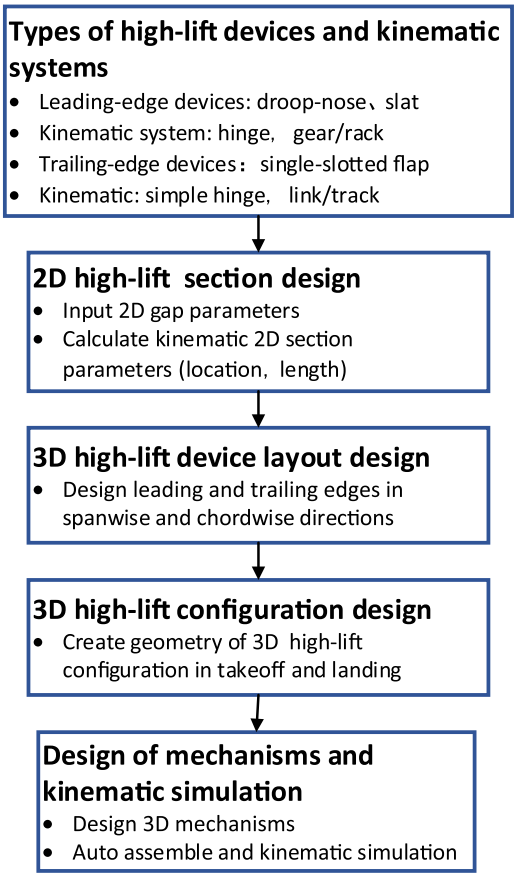

Fig. 20. Aerodynamic mechanism–integrated design process of a high-lift system

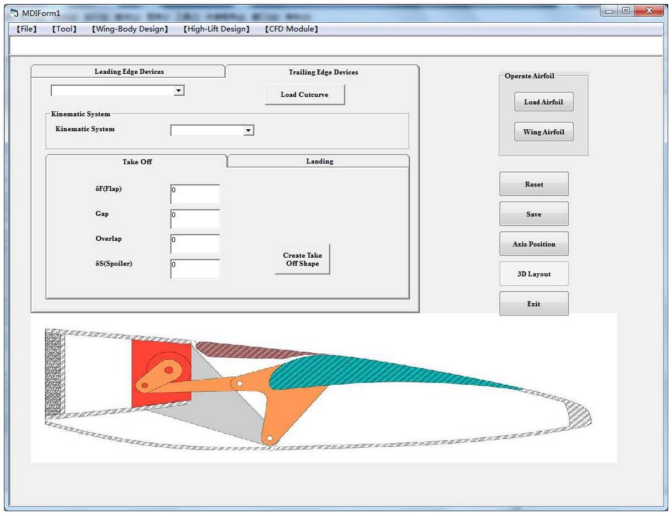

Fig. 21. Two-dimensional high-lift section design module

based on the cruise wing shape, this platform integrates the design of the wing–body and high-lift system together.

The work in the high-lift device design finalization phase includes generating a 3D geometry model based on a 2D multielement airfoil and designing a driving mechanism system to deploy the high-lift devices to the position designated by aerodynamic designers.

The traditional design method may face a serious problem in this phase. The work involved in the multielement airfoil design phase involves primarily optimizing gap parameters to obtain the optimum aerodynamic characteristics. The optimal gap parameters of takeoff and landing obtained via optimization are hardly achieved by reasonable mechanical devices. Thus, negotiation and compromise between aerodynamic and mechanical designers may occur.

For the aforementioned reasons, a new principle for high-lift system design was formulated. The kinematic type and mechanism size of a high-lift device are determined first, then the aerodynamic characteristics of the high-lift device based on the kinematic system are optimized. This principle integrates aerodynamic and mechanical design, as illustrated in Fig. 20.

Two-Dimensional High-Lift Section Design

In this module, a multielement airfoil is designed based on a clean airfoil according to the gap parameters and deflection angles, which can be input from the software interface, as shown in Fig. 21. The clean airfoil can be loaded from an airfoil data file or cut out from a clean wing model at the designated spanwise position. The cone of the leading-edge slat and the nose of the trailing-edge flap is cut out from the clean airfoil by shape curves that can be input as data points or manually designed via *CATIA*.

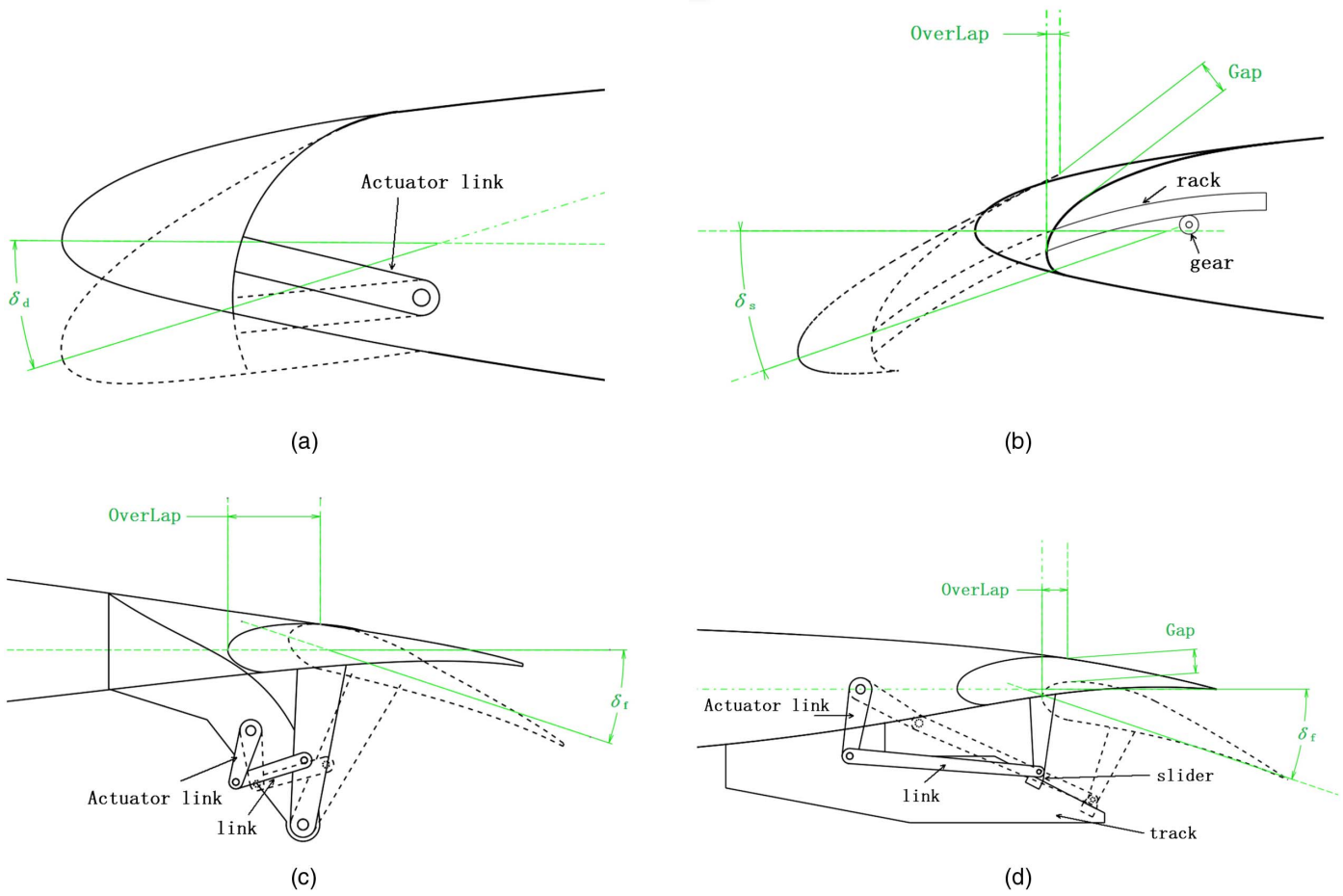

Fig. 22. (a) Leading-edge droop-nose mechanism; (b) leading-edge slat mechanism; (c) trailing-edge flap simple hinge mechanism; (d) trailing-edge flap link-track mechanism

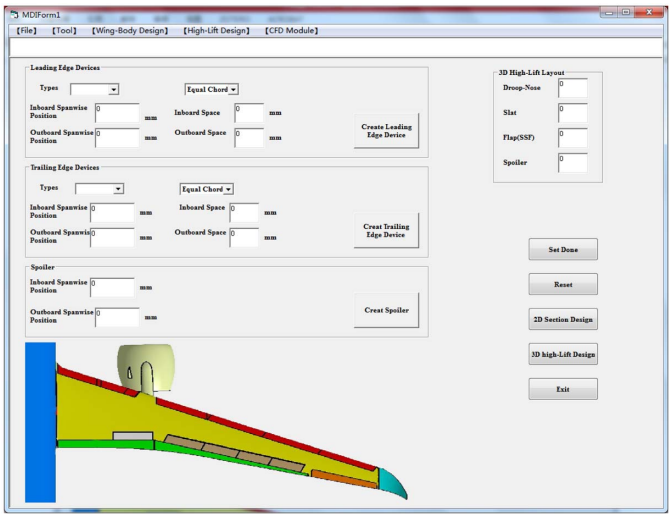

Fig. 23. Interface for 3D high-lift device layout design module

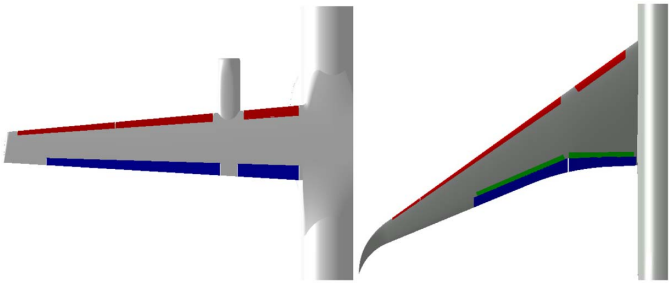

Fig. 24. Two different layout designs of high-lift devices on different wings

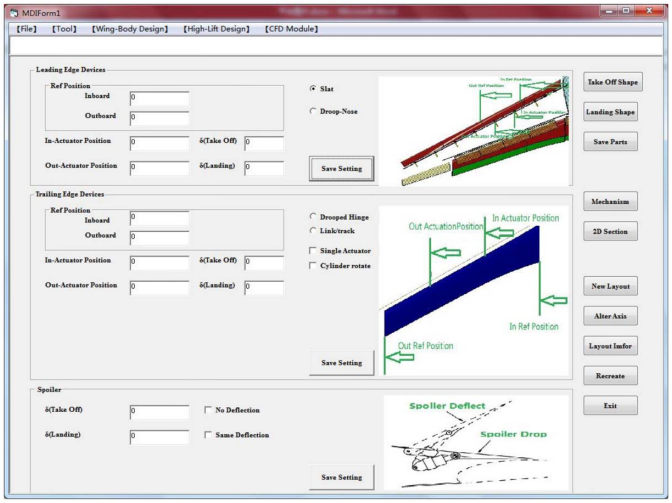

Fig. 25. Three-dimensional high-lift devices for takeoff and landing configuration design module interface

The kinematic system should be selected before the aerodynamic/mechanical integrated design is carried out. For example, if the trailing-edge device single-slotted flap (SSF) is deployed on a simple hinge that provides a circular deployment to the flap, both the takeoff and landing configurations will be deployed in a circular motion. The position of the hinge will be determined when the gap parameters of takeoff or landing status are defined, then the gap and overlap of another status is controlled by the deflection angle. The gap and overlap will then be calculated and displayed to the designer to facilitate the design.

As illustrated in Fig. 22, the droop nose and gear/rack for leading-edge device kinematic systems and simple hinge and link/track for trailing-edge device kinematic systems can be selected as candidates.

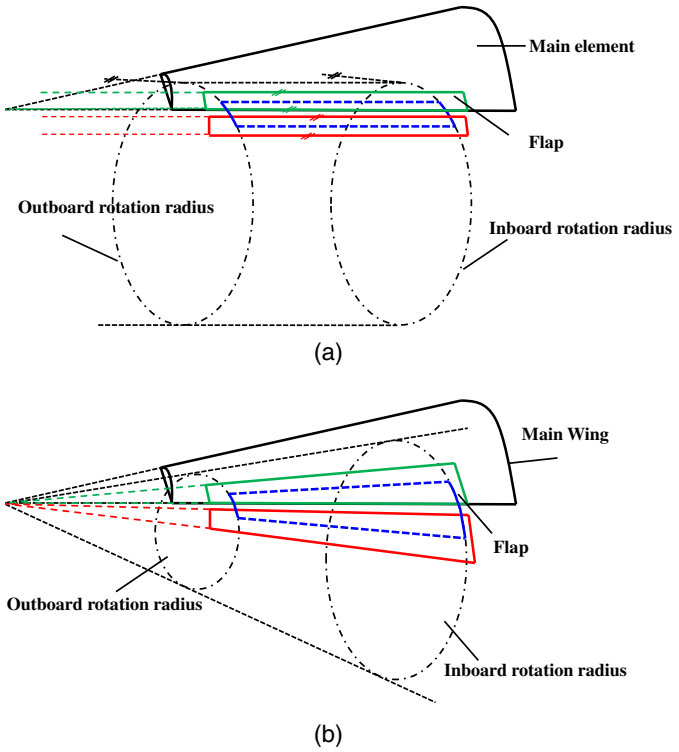

Fig. 26. (a) Trailing-edge flap cylinder rotation; (b) trailing-edge flap cone rotation

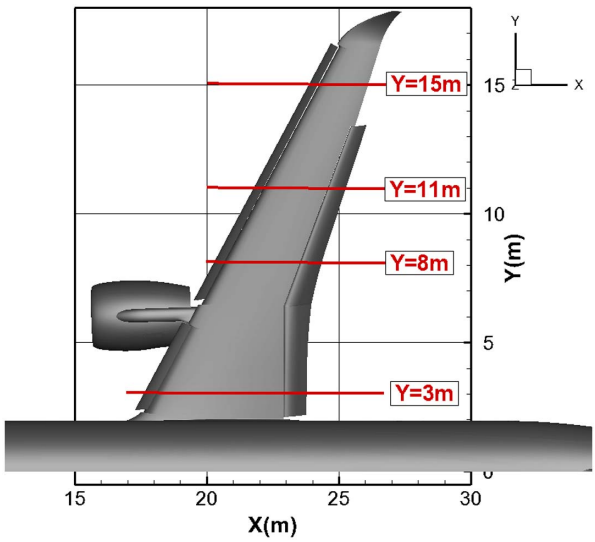

Fig. 27. Landing configuration of 150 seat airliner

Three-Dimensional High-Lift Device Layout Design

The interface for a 3D high-lift device layout design module is shown in Fig. 23. The types of high-lift devices are determined via this interface as well as the relative chord length, relative spanwise length, and location of the leading and trailing edges of the high-lift device. Here, the software allows different devices to be deployed at any position of the wing, with no limitation on the number and location of the high-lift devices. The different designs displayed in Fig. 24 show that the software has wide applicability.

Three-Dimensional High-Lift Devices for Takeoff and Landing Configuration Design

Three-dimensional high-lift devices for takeoff and landing configurations can be generated after a high-lift device layout is designed, as depicted in Fig. 25. The takeoff and landing configurations are deployed via the selected kinematic system and position of operational mechanisms.

Because the spanwise movement and rotation along the leading-edge wing are not the same, achieving a 3D high-lift configuration that matches the 2D gap parameters is almost impossible. Three-dimensional high-lift devices are determined by the design parameters on two sections along the span direction. By transiting the 2D mechanical parameters onto the two sections, a high-lift device can be defined. Three-dimensional high-lift devices approach the 2D design at two standard sections to the highest possible extent. Based on the kinematic system types and the position of the operational mechanisms, the kinematic parameters of the mechanisms and high-lift devices on the mechanical plane can be calculated according to rigid body dynamics.

The real space rotation of leading- and trailing-edge devices is divided into cylinder rotation and cone rotation, respectively. Cylinder rotation is rotation in which the rotation radius is equal along the rotation axis. Conversely, the rotation radius is not equal along the rotation axis in the cone rotation, as illustrated in Fig. 26. If the actuator axes of two operational mechanisms are not in the same line, there is lateral rotation along the same trajectory as the

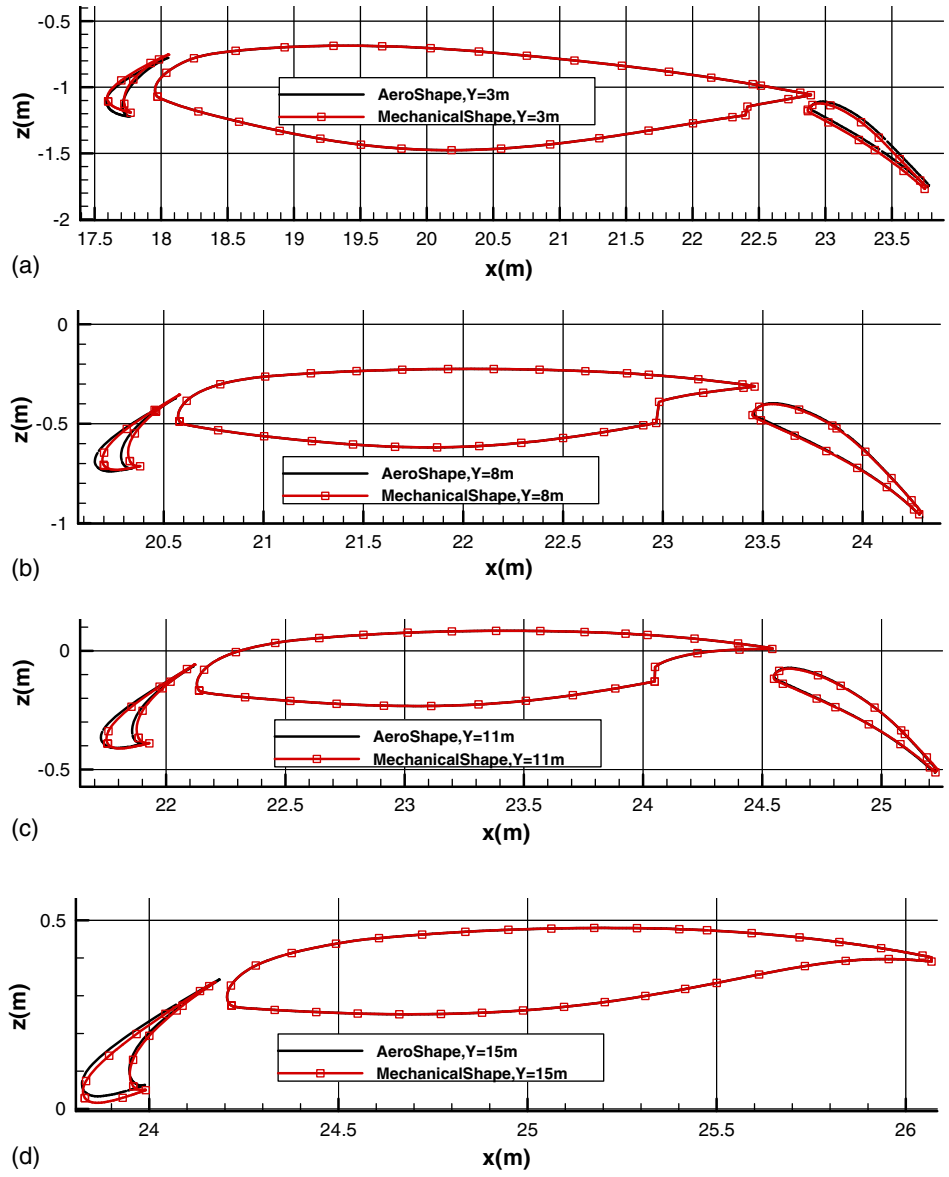

Fig. 28. Spanwise cross-section profile comparison between aerodynamic and mechanical drive shape: (a) Slice Y = 3 m; (b) Slice Y = 8 m; (c) Slice Y = 11 m; (d) Slice Y = 15 m

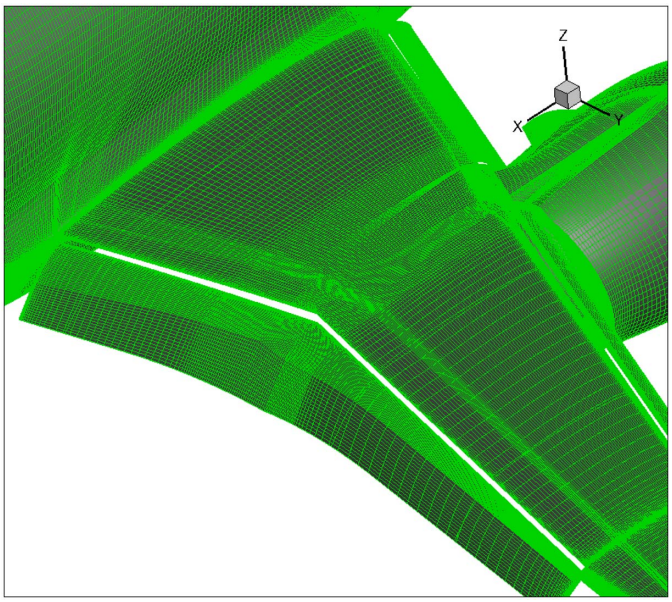

Fig. 29. Wing–body surface structure mesh

high-lift device's movement. In practice, this lateral rotation is limited by a kinematic pair connected between the mechanism and the high-lift device. The position, approach, and constraint direction of the kinematic pair are directly related to the final position of the high-lift devices, and the reverse process is difficult to achieve.

Fig. 27 shows the landing configuration model (with nacelle, wingtip, and empennage designed manually) of a 150 seat airliner designed by the software. Here, the leading-edge device is deployed on circular gear/rack devices, with equal chord length along the span. The inboard trailing edge device is SSF with equal chord length along the span and deployed on a simple hinge deflecting according to the cylinder rotation. The outboard trailing-edge device is SSF with equal relative chord length along the span and deployed on two simple hinge mechanical systems deflecting according to the cone rotation.

Fig. 28 compares the cross-section profiles at different spanwise positions between the initial aerodynamic configuration (aero shape) and the configuration derived by the mechanical systems (mechanical shape) based on the aerodynamic shape, and the detailed spanwise positions are marked in Fig. 27. As can be seen from Fig. 28, there exist some differences between the aero shape and mechanical shape on the leading-edge slat, and the difference in the trailing-edge flap is mainly on the inboard.

Fig. 29 presents the surface structure mesh generated manually. Fig. 30 compares the aerodynamic performance of the aero shape and mechanical shape. It can be seen that there only exists minor differences at large angles of attack.

Mechanism Design and Kinematic Simulation

After all parts are completed, assembly and kinematic simulation can be performed using the software with the Digital Mock-Up (DMU) module of *CATIA*. In addition, the parts under manipulation can be output by the software. In the DMU module, the kinematic characteristics can be tested. By analyzing the data and regulations, designers are then able to come up with better schemes. Figs. 31 and 32 show the effects of the kinematic simulation.

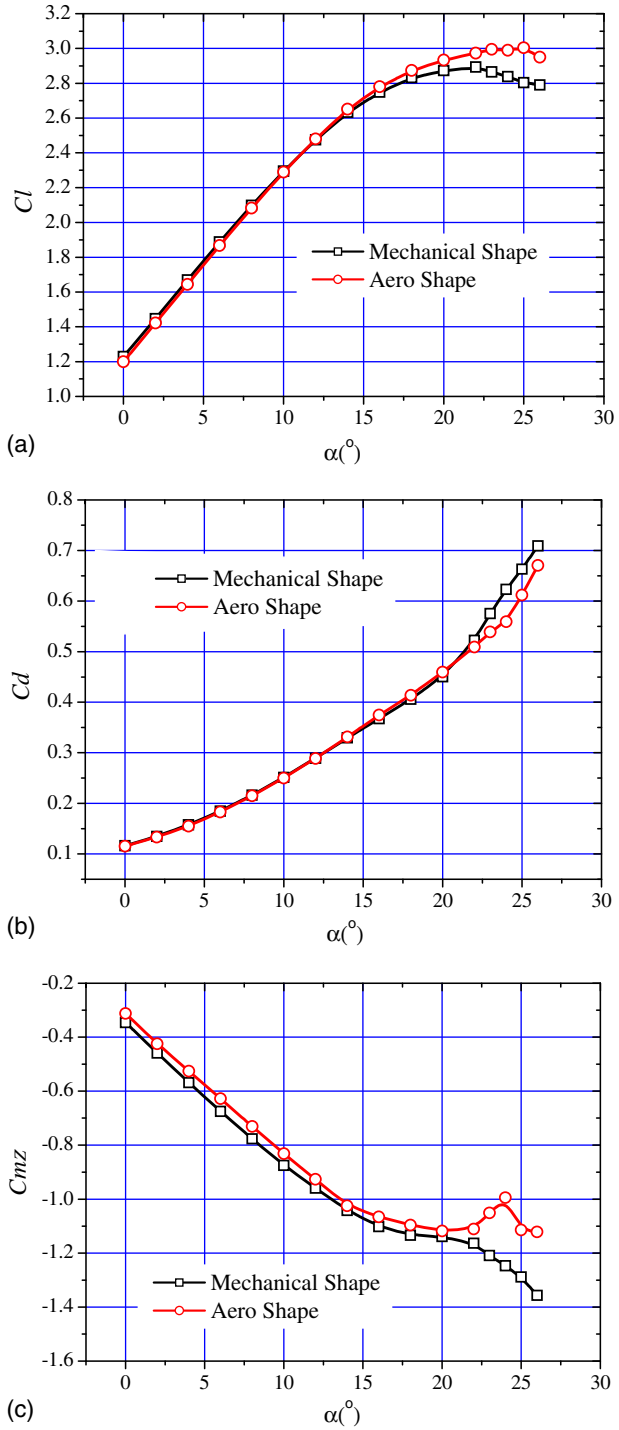

Fig. 30. Aerodynamic characteristic comparison between aerodynamic shape and mechanical drive shape: (a) lift coefficient curve; (b) lift coefficient curve; (c) lift coefficient curve

Conclusion

In this paper, a software using VB 6.0 for wing–body parametric modeling and high-lift system design was developed. This software integrates parametric modeling and the design of control curves (i.e., airfoils), fuselage design, wing design, aerodynamic computation of the airfoil and wing–body combination, and 3D high-lift and mechanical design.

NACA0012 airfoil and DLR-F6 WB FX2B wing–body models were selected to verify the geometric modeling and aerodynamic

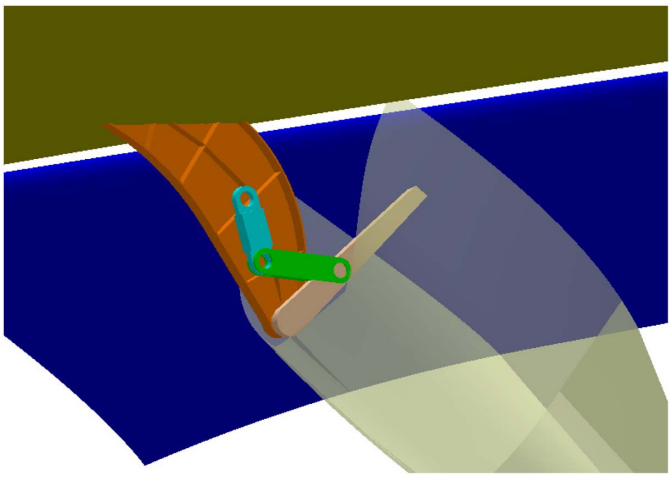

Fig. 31. Trailing-edge simple hinge mechanisms

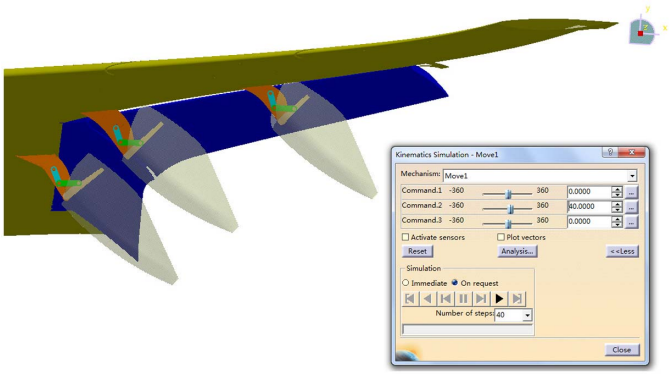

Fig. 32. DMU kinematic simulation

numerical computation functions. The results demonstrate that the accuracy of the airfoil fitting and wing–body CAD model are acceptable and the numerical computation method is reliable.

Based on the cruise configuration model (with nacelle, wingtip, and empennage designed manually) of a 150 seat airliner designed using this software, two different landing configurations were designed. One describes the aerodynamic performance (aero shape) and the other was derived by the mechanical systems (mechanical shape) based on the aero shape. The results show that there exist some minor differences in the geometrical and aerodynamic performances both on the leading-edge slat and the trailing-edge flap. Based on the mechanical shape, a high-lift driving mechanism was designed and the driving mechanism motion was simulated. The results illustrate that the software was able to integrate wing–body modeling and high-lift aerodynamic/mechanical design in the conceptual and preliminary aircraft design phases.

Notation

The following symbols are used in this paper:

C_D = drag coefficient (reference length: chord);
C_L = lift coefficient (reference length: chord);
C_M = pitching moment coefficient;
C_p = pressure coefficient;
c = airfoil chord;
M = Mach number;
R = Reynolds number; and
α = angle of attack (degrees).

References

Anemaat, W. A., and Schueler, K. L. (1997). "Airplane configuration layout design using object-oriented methods." *AIAA Paper 97:5510*, World Aviation Congress, Anaheim, CA.

CADS [Computer software]. Open Mind Technologies AG, Wessling, Germany.

Fidanci, M., Miller, J. R., and Strauss, D. J. (2000). "Integrating automated multi-disciplinary optimization in preliminary design of non-traditional aircraft." *ADA380252*, Air Defense Agency, Wright-Patterson Air Force Base, OH.

Head, H., Carolina, S., and Raymer, D. P. (1992). "RDS: A PC-based aircraft design, sizing, and performance system." *AIAA 92-4226*, Guidance, Navigation and Control Conference, Hilton Head Island, SC.

Jayaram, S., Myklebust, A., and Gelhausen, P. (1992). "ACSYNT-A standards-based system for parametric, computer aided conceptual design of aircraft." *AIAA 92-1268*, Aerospace Design Conference, Irvine, CA.

Liu, H. M. (2010). *Programming of visual basic case tutorial*, Posts and Telecom Press, Beijing.

Lu, X. L., and Gong, X. D. (2008). "Development research of aircraft synthetic conceptual design software." *Third Chinese Society of Aeronautics and Astronautics Youth Science and Technology Forum*, Chinese Society of Aeronautics and Astronautics, Beijing, 3–14.

Manning, T. A., et al. (2004). "ComGeom2: A geometry tool for multidisciplinary analysis and data sharing." *10th AIAA/ISSMO Multidisciplinary Analysis and Optimization Conf., AIAA-2004-4303*, American Institute of Aeronautics and Astronautics, Albany, NY.

OpenCADS [Computer software]. Open Mind Technologies AG, Wessling, Germany.

OpenFOAM [Computer software]. OpenFOAM Foundation, London.

Painchaud-Ouellet, S., Tribes, C., Trepanier, J. Y., and Pelletier, D. (2004). "Airfoil shape optimization using NURBS representation under thickness constraint." *42nd AIAA Aerospace Sciences Meeting and Exhibit, AIAA 2004-1095*, American Institute of Aeronautics and Astronautics, Reno, NV.

Sclafani, A. J., Vassberg, J. C., Harrison, N. A., Rumsey, C. L., Rivers, S. M., and Morrison, J. H. (2008). "CFL3D/OVERFLOW results for DLR-F6 wing/body and drag prediction workshop wing." *J. Aircr.*, 45(3), 762–780.

Shi, F. Z. (2001). *Computer-aided geometric design and non-uniform rational B-spline*, Higher Education Press, Beijing, 211–245.

Wang, Y. C. (2013). "Research on B-spline parameterization of supercritical wings." M.Sc. dissertation, Beihang Univ., Beijing.

Xie, X., and Haberland, C. (1999). "A new numerical design tool for concept evaluation of propeller aircraft." *Aircr. Des.*, 2(3), 147–165.

Xie, Y. F., and Yu, X. Q. (2008). "Parametric design of aircraft configuration using API in CATIA." *Comput. Eng. Des.*, 29(14), 078.

Zhan, L., Yu, X. Q., and Sheng, Q. (2009). "Parametric CAD model of aircraft configuration for civil jets conceptual design." *Comput. Eng. Des.*, 30(16), 3887–3890.

Zhang, X. J. (2002). *Aircraft design manual VI—Aerodynamic design*, Aviation Industry Press, Beijing, 51–52.